ACS OMEGA

http://pubs.acs.org/journal/acsodf

Article

# Speciation and Semiquantification of Nitrogen-Containing Species in Complex Mixtures: Application to Plastic Pyrolysis Oil

Charlotte Mase, Julien Florent Maillard, Benoit Paupy, Marie Hubert-Roux, Carlos Afonso,* and Pierre Giusti

Cite This: *ACS Omega* 2022, 7, 19428−19436

Read Online

ACCESS | Metrics & More | Article Recommendations | Supporting Information

**ABSTRACT:** Plastic pyrolysis oil is of particular interest for waste management in the current context of a circular economy. Due to their uncontrolled origin, these oils may contain significant amount of unwanted compounds such as nitrogen-containing species. These compounds are known to be catalyst poisons during refining processes. Therefore, the removal of these species is crucial, and their characterization from structural and quantification points of view is essential for this purpose. This study presents a method to specify and quantify nitrogen-containing classes in a plastic pyrolysis oil by direct infusion mass spectrometry. Two steps were used, namely structural characterization to select suitable standards and semiquantification. The structural speciation of nitrogen-containing compounds was first performed by electrospray ionization Fourier transform mass spectrometry, followed by tandem mass spectrometry using high-resolution mass isolation and infrared multiphoton dissociation fragmentation. A semiquantification is then performed by the standard addition method, which is very appropriate for such complex matrices. Aromatic cores such as quinoline and quinoxaline were evidenced for both $N_1$ and $N_2$ classes, allowing 2-methylquinoxaline and 2-butylquinoline to be proposed as standards for the semiquantification of $N_2$- and $N_1$-containing compounds, respectively. The amount of nitrogen detected from the sum of the individual species was consistent with the bulk analysis. The reported methodology can be applied to numerous other families of compounds in various other complex matrices.

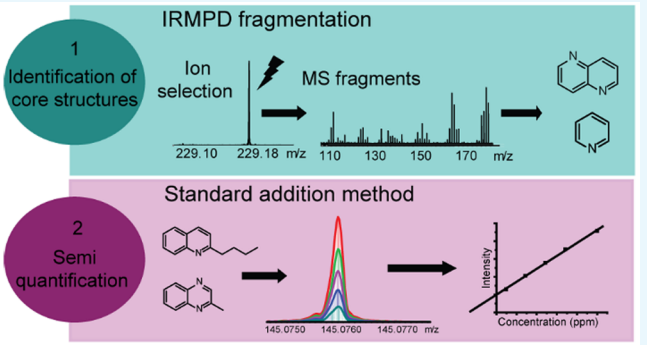


## INTRODUCTION

Over the past decade, the production of plastic has steadily increased due to its applications in many sectors. Since the start of their large-scale production in 1950, nearly 9 billion tons of plastics have been manufactured from petroleum. Of the high amount of plastic waste generated, only around 9% is currently recycled.[1] As a consequence, if this production and waste management continue, around 12 million tons of plastic waste will end up in landfills or in the natural environment by 2050.[2] The current trend is therefore towards a circular economy, which represents a more sustainable alternative model to the linear economy.[3−5] Plastic depolymerization is a very promising strategy in this context.[6] Through such a process, the recovery of monomers, the basic chemical units of polymeric chains, transforms plastic from a waste product to a new precursor material. Thermal treatments are used to degrade these polymeric chains.[7−9] Pyrolysis is one of the different types of chemical degradation processes that occur at high temperatures in the absence of oxygen.[10,11] It is mainly used in the valorization of organic materials[12] such as biomass,[13−15] polymers,[16−19] or plastics[20−22] and allows the production of solid (coal), liquid (oil), and gaseous (non-condensed gases) products. Each was previously characterized using different analytical methods such as gas chromatography (GC),[21,23−26] infrared spectroscopy (IR),[27] nuclear magnetic resonance (NMR),[19] and mass spectrometry (MS).[12,16,25] Because pyrolysis oil is of particular interest for the recovery of monomers, the material chosen in this study is a pyrolysis oil produced from real municipal wastes made up of different plastic types. Owing to the high molecular complexity of such samples, the necessity of using very-high-resolution mass spectrometry such as Fourier transform ion cyclotron resonance (FTICR) to characterize plastic oils has been demonstrated.[12,25,28] Specifically, in a previous study, the presence of nitrogen-containing species in the plastic pyrolysis oil was highlighted by electrospray ionization (ESI).[29] Nitrogen-containing species form due to the presence of

Received: February 24, 2022
Accepted: April 6, 2022
Published: June 3, 2022

antioxidant additives such as hindered amine light stabilizers (HALS) and nitrogen-containing polymers such as polyamides in the plastic waste. These nitrogen-containing molecules are of particular interest because they can act as catalyst poisons during refining processes. The elemental analysis of this sample showed the presence of 1797 ppm of nitrogen. A gas chromatograph coupled with a nitrogen chemiluminescence detector (GC-NCD) was used to show that of this 1797 ppm N, 300 ppm was speciated into benzonitrile and caprolactame molecules. Nevertheless, more than 850 signals of nitrogenated species were detected by electrospray ionization (ESI) in the positive mode. Less than 100 signals with low intensities were observed via ESI in the negative mode and were therefore not included in this study. The present challenge is to quantify these species to determine if their concentrations explain the missing 1497 ppm nitrogen. However, the structures of these compounds are unknown, and mass spectrometry quantification implies the use of a standard to take into account differences in the ionization efficiency. For this purpose, the first step of this work was the structural characterization of the nitrogen-containing species to select standard compounds representative of the species present in the sample.

One way to access structural information is tandem mass spectrometry (MS/MS).[30−34] For this, ions of interest were isolated, typically with a quadrupole, and fragmented afterward through collisional activation. However, in the case of a complex mixture and because of the low resolution delivered by the quadrupole, MS/MS spectra can be difficult to interpret.[35,36] On FTICR mass spectrometers, however, it is possible to perform high-resolution mass selection directly in the ICR cell using frequency-specific excitation pulses.[37]

The second step is quantification. In practice, as with most "detectors", the signal in ESI-MS is proportional not only to the concentration but also to the analyte response factor. Calibration with standard molecules is therefore necessary. Different methods of calibration are reported in literature, such as internal calibration,[38] external calibration,[39] and the standard addition method (SAM),[40] depending on the desired requirements. In the case of a highly complex mixture that may yield a strong matrix effect and that already contains most possible molecular formulas, the SAM is the method of choice. The calibration is carried out directly in the sample. The matrix will be analyzed alone and then with known supplemental additions of the substance to be measured. Such a procedure is usually used with separation methods such as liquid or gas chromatography. However, in the case of ultracomplex mixtures such as bio-oils,[41−43] plastic pyrolysis oils,[12] and other mixtures,[44,45] the huge amount of different isomers may yield a very low concentration per molecule. The use of direct infusion mass spectrometry (DI-MS) can remove the isomeric dispersion and thus very significantly improve the detection limit per molecular formula.

In the present work, we report the structural analysis of basic nitrogen-containing compounds in a mixed-plastic pyrolysis oil from real municipal waste by DI-ESI(+)-FTICR MS/MS using infrared multiple photon dissociation (IRMPD). A relative quantification is also reported through the use of different standards containing the main nitrogen-containing cores that were evidenced.

## MATERIALS AND METHODS

**Sample and Reagent.** The mixed-plastic pyrolysis oil was supplied by TotalEnergies TRTF (TotalEnergies Total Research and Technology Feluy, Belgium). Toluene, methanol, and heptane of analytical grade with purities higher than 99.7% were all purchased from VWR. 2-Butylquinoline and 2-methylquinoxaline were purchased from Sigma-Aldrich.

**Sample Preparation.** The stock solution of pyrolysis oil was prepared at a concentration of 5 mg $mL^{-1}$ in toluene. For tandem mass spectrometry, the sample was further diluted to a concentration of 0.5 mg $mL^{-1}$ in toluene/methanol (50:50 v/v) and doped with 1% formic acid. For the SAM, the pyrolysis oil solution was prepared at a concentration of 0.5 mg $mL^{-1}$ in toluene/methanol (50:50 v/v). The standard solution (of 2-methylquinoxaline or 2-butylquinoline) was prepared at a concentration of 1 mg $mL^{-1}$ by the gravimetric method and further diluted to a concentration of 1 $\mu$g $mL^{-1}$. These solutions were prepared three times to avoid systematic error dilution propagation on all points of the range. The dilutions of the solutions were carried out by the volumetric method. Volumes used of each solution for a total volume of 1 mL are reported in Table S1. Five-point calibration was used with a concentration range between 0.005 and 0.025 $\mu$g $mL^{-1}$. Triplicates were made and registered for each case.

**Mass Spectrometry Analyses.** FTICR experiments were performed using a 12 T SolariX XR MRMS (Bruker Daltonics, Bremen, Germany) instrument. Samples were ionized using an ESI source in the positive mode with a flow rate of 120 $\mu$L $h^{-1}$. The mass spectrometer was externally $m/z$ calibrated using a trifluoroacetate solution before sample analysis. Source parameters were chosen as follows: capillary voltage of 3900 V, source temperature of 370 °C, desolvatation gas flow of 4 L $min^{-1}$, nebulizer pressure of 2 bar, quadrupole lower cutoff of 100, and TOF of 0.7 ms. For the IRMPD parameters, a 30 W 10200−10800 nm IR laser (Synrad 48-1) was used at a laser power of 75% and a laser irradiation time of 2 s. A mass range of $m/z$ 73−1000 with a 1.2 transient length was selected, resulting in a resolution of 230 000 at $m/z$ 400. The number of scans averaged was 200 for infusion and 20 for IRMPD fragmentation to keep the ICR cell from overheating. Instrument control and data acquisition were performed using the FTMS control (ver. 2.3, Bruker) software.

**Data Processing.** For FTICR experiments, data were processed with DataAnalysis (ver. 5.1, Bruker). A unique molecular formula could be attributed to each $m/z$ signal with a signal-to-noise ratio (S/N threshold) >6 thanks to the mass accuracy and the resolving power of FTICR. Raw formulas $O_{0-4}-N_{0-3}$ and $N_{0-2}$ for were picked broadband analysis and MS/MS experiments, respectivelyto avoid misassignment. For double bond equivalent (DBE) versus carbon number plot used to visualize the data sets, the degree of unsaturation (DBE) was calculated using eq 1, where $n_C$ is the number of carbon atoms, $n_H$ is the number of hydrogen atoms, and $n_N$ is the number of nitrogen atoms.

$$\mathrm{DBE} = n_C - \frac{n_H}{2} + \frac{n_N}{2} + 1 \quad (1)$$

## RESULTS AND DISCUSSION

In a previous study, thanks to the ability of positive-ion electrospray ionization (ESI(+)) to promote the ionization of basic molecules, the nitrogen-containing species were distinguished by ESI(+)-FTICR[29] as shown in Figure 1a, which presents the mass spectrum of this plastic pyrolysis oil in ESI(+)-FTICR-MS. Both the $N_1$ and $N_2$ classes of compounds represent an abundance of more than 40% of the total



https://doi.org/10.1021/acsomega.2c01114
ACS Omega 2022, 7, 19428−19436

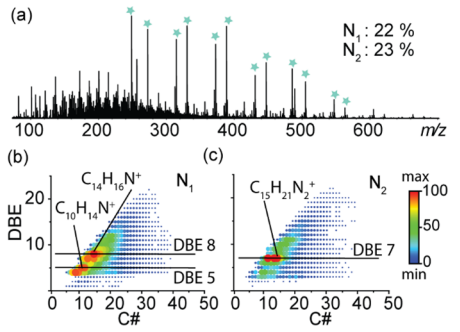


**Figure 1.** (a) Mass spectrum of the plastic pyrolysis oil obtained via ESI(+). DBE vs carbon number plots for (b) the $N_1$ family and (c) the $N_2$ family (stars for polypropylene glycol contaminant).

attributed number of ions with assigned molecular formulas of 405 and 444, respectively. DBE versus carbon number plots of these molecular classes are given in Figure 1b and c. Two main distributions at DBE = 5 and 8 were observed for the $N_1$ family, whereas only one major distribution at DBE = 7 was observed for the $N_2$ family. Distributions are included between 4 and 40 carbon atoms with the $CH_2$ horizontal gap. Given the high number of species, it is necessary to find molecules representative of the species present in the sample to be used as standards. In such matrices, a continuum has been observed inside distributions with a same core and a $CH_2$ repetitive unit.[46,47] Based on this knowledge, three intense ions will be selected with molecular formulas of $C_{10}H_{14}N^+$ (DBE = 4), $C_{14}H_{16}N^+$ (DBE = 8), and $C_{15}H_{21}N_2^+$ (DBE = 7).

**Identification of Core Structures.** In the case of such a complex mass spectrum, the low resolution for mass selection afforded by the quadrupole induces the coisolation of many isobaric ions. More than 15 isobaric ions are coisolated, with an isolation window of 1 Da (Figure S1). Among these ions, several belong to $N_2$, $N_2O$, and $N_2O_2$, where DBE = 7, 8, and 9, respectively. In petroleum compounds that have survived geological times, there are a few constraints concerning their possible core structures. In the present case, it is much more difficult to predict the molecular structure consistent with a particular molecular formula. In particular, we do not know whether heteroatoms are located in the aromatic core and thus

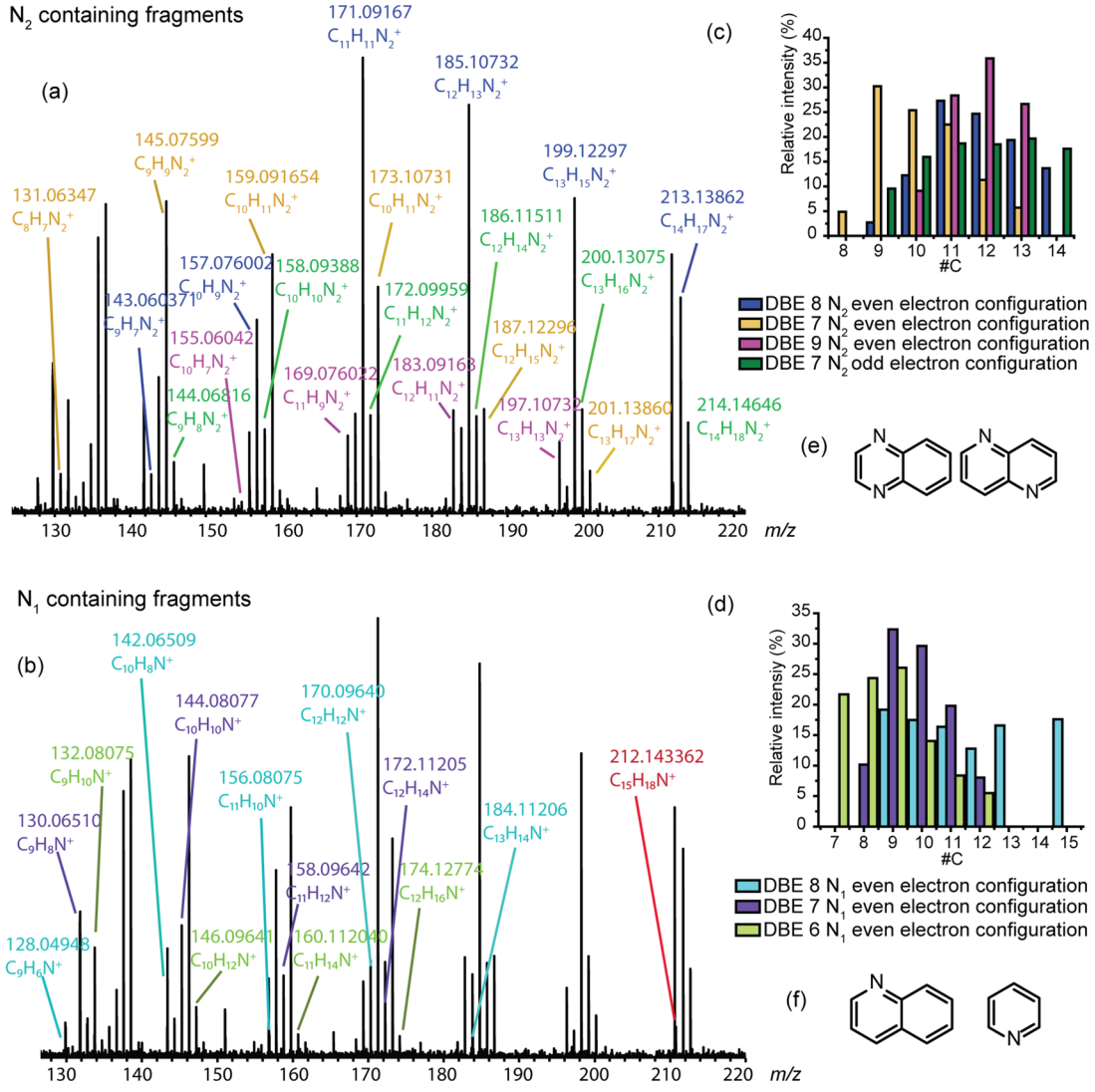


**Figure 2.** Fragmentation mass spectrum obtained via IRMPD for the $C_{15}H_{21}N_2^+$ ion at $m/z$ 229.169925 attributed to (a) $N_2$-containing fragments and (b) $N_1$-containing fragments. Carbon number distribution of (c) $N_2$-containing fragments and (d) $N_1$-containing fragments. Putative cores structures for (e) $N_2$-containing fragments and (f) $N_1$-containing fragments.



https://doi.org/10.1021/acsomega.2c01114
ACS Omega 2022, 7, 19428−19436

whether $N_2O$ or $N_2O_2$ precursors that were coisolated with the interest precursor ion $C_{15}H_{21}N_2^+$ during collision-induced dissociation (CID) will give $N_2$ fragments that will compromise the attribution of fragments. To avoid such problems, ICR cell isolation was perfromed at high resolution, followed by IRMPD fragmentation. Only one species was selected, as seen in Figure S1. The DBE versus carbon number plot therefore shows only a single point to avoid misinterpretation. Comparisons between quadrupole and in-cell isolation for $C_{10}H_{14}N^+$ (DBE = 4) and $C_{14}H_{16}N^+$ (DBE = 8) are given in Figures S2 and S3, respectively.

$C_{15}H_{21}N_2^+$ was the most abundant ion of the $N_2$ family. It had a DBE value of seven, which may correspond to an aromatic structure. Its fragmentation spectrum is reported in Figure 2. Eight fragmentation series were identified. To facilitate interpretation, the attributions of each series are presented in different colors. These series were classified into two families: fragments containing two nitrogen atoms (Figure 2a) and fragments containing one nitrogen atom (Figure 2b). Most fragments contained two nitrogen atoms, and their DBE values were located between seven and eight (Figure S4). Fragments with only one nitrogen have the lowest DBE values of six and seven and present low $m/z$ values. This suggests that both nitrogen atoms were mainly present in a fused aromatic core.

Panels c and d in Figure 2 represent the carbon number distributions for each series of the $N_1$ and $N_2$ fragments, respectively. The blue and green series of the $N_2$-containing fragments present the same fragmentation pattern, with carbon numbers between 8 and 14. Blue is composed of ions with even electron configurations, and green is composed of ions with odd electron configurations. The presence of radical fragment ions is possible thanks to the presence of aromatic rings in the precursor ion that can stabilize the radical with a mesomeric effect. However, the DBE value was not the same between both fragmentation series. Indeed, during charge-driven fragmentation, a proton migration occurs that leads to an increment of one DBE.[48,49]

Two putative structures in agreement with the experimental data related to the $C_{15}H_{21}N_2^+$ ion precursor are given in Figure 2e. The structures involve aromatics with two fused aromatic six-membered rings with two nitrogen atoms included in the core, such as naphthyridine or quinoxaline. However, it is impossible to know if nitrogen atoms were present in the same cycle or separated. The two other $N_2$ series (yellow and pink) also involve charge-driven dissociation mechanisms. Fragments of the pink series had a DBE value of nine and included carbon numbers between 13 and 10. The first fragment ion of this series was produced through the loss of two $CH_4$ molecules, whereas the first fragment ion of the yellow series was produced through the loss of $C_2H_4$. These ions, in the same manner as the green and blue series, were followed by a series of fragment ions separated by $CH_2$ units. It should be pointed out that such fragment ion series are not expected to be consecutive fragments. They are rather due to (i) the existence of numerous isomers that can fragment differently depending on the alkyl chain length and (ii) competitive fragmentations within a particular isomer yielding, for instance, the loss of alkanes such as methane and ethane.

The DBE = 9 series that presents an increase of two DBE values compared to the precursor ion could be due to fragments presenting a double bond outside the aromatic core after an internal rearrangement stabilized by the mesomeric effect. The yellow series has a DBE value of seven, and between 8 and 13 carbon atoms were included. The same type of fragmentation as that for the pink series was retrieved, but neither double bond outside the cycle was present. However, a DBE value of seven could be explained by a rearrangement during the fragmentation and the loss of aromaticity. Nevertheless, a core proposal of two fused aromatic six-membered rings with two nitrogen atoms included was thus demonstrated.

For the second class of fragmentation of the $C_{15}H_{21}N_2^+$ ion, the $N_1$-containing fragmentation series (purple, red, light blue, and light green) present even electron configurations. A single fragment (in red) indicated the loss of $NH_3$ that could be attributed to an amine end-group in the precursor ion. A series of fragment ions were produced by the loss of $NH_3$ in addition to an alkyl group (light blue color), which is characteristic of nitrogen being present in the ramified chain and not in the extremity. However, a core composed of two fused aromatic six-membered rings was proposed, such as quinoline (Figure 2f). For the purple and light green series, the last fragments contain a carbon number of seven. Thus, the proposed structure for the core of these series was composed of one fused aromatic six-membered ring such as pyridine with an unfragmented alkyl chain (Figure 2f).

The same procedure was applied for both $N_1$ species $C_{10}H_{14}N^+$ (DBE = 4) and $C_{14}H_{16}N^+$ (DBE = 8). Results are reported in the Supporting Information. For the $N_1$ fragmentation results, quinoline or pyridine aromatic cores could be proposed as representative of the molecules present in the pyrolysis oil.

**Semiquantification by the Standard Addition Method.** As announced before, it is impossible to find all standard molecules to perform the SAM given the number of species in the plastic pyrolysis oil. Two representative standards were purchased for semiquantification by the SAM according to the fragmentation results. Structures of 2-butylquinoline and 2-methylquinoxaline, which were selected to quantify the $N_1$ and $N_2$ species, respectively, are given in Figure 3. The hypothesis done in this study is that all $N_1$-containing species have the same response factors, and the same is true for all $N_2$-containing species in positive ESI mode.

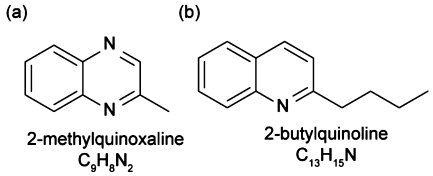


**Figure 3.** Standard chemical structures of (a) 2-methylquinoxaline and (b) 2-butylquinoline

Figure 4a presents the SAM procedure, including four main steps: (i) the addition of known volumes of standard to the sample, (ii) the analysis of these samples, (iii) graphical representation, and (iii) mathematical correlation. A minimum of three points are required for the SAM,[50] and the concentrations included are typically between 0.5 and 4× the analyte concentration.[51,52] The center of the standard range must correspond to the concentration of the analyte in the matrix without standard addition. Moreover, it is necessary to ensure that the concentration range chosen is in the linearity


https://doi.org/10.1021/acsomega.2c01114
ACS Omega 2022, 7, 19428−19436

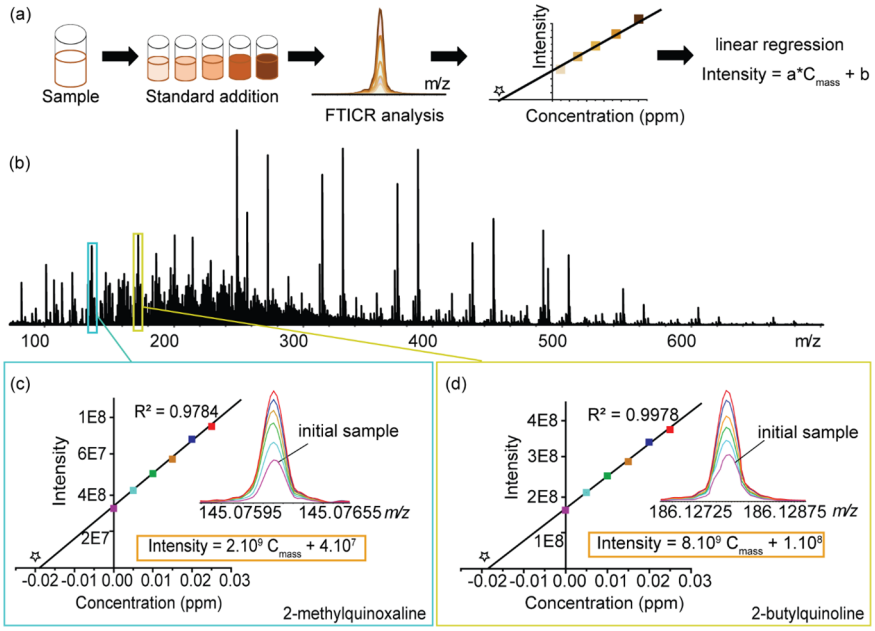


**Figure 4.** (a) Methodology of the SAM and its application to plastic pyrolysis oil. (b) Mass spectrum of plastic pyrolysis oil obtained via ESI(+)-FTICR, with enlarged insets showing (c) the 2-methylquinoxaline standard addition and its intensity versus concentration plot and (d) the 2-butylquinoline standard addition and its intensity versus concentration plot.

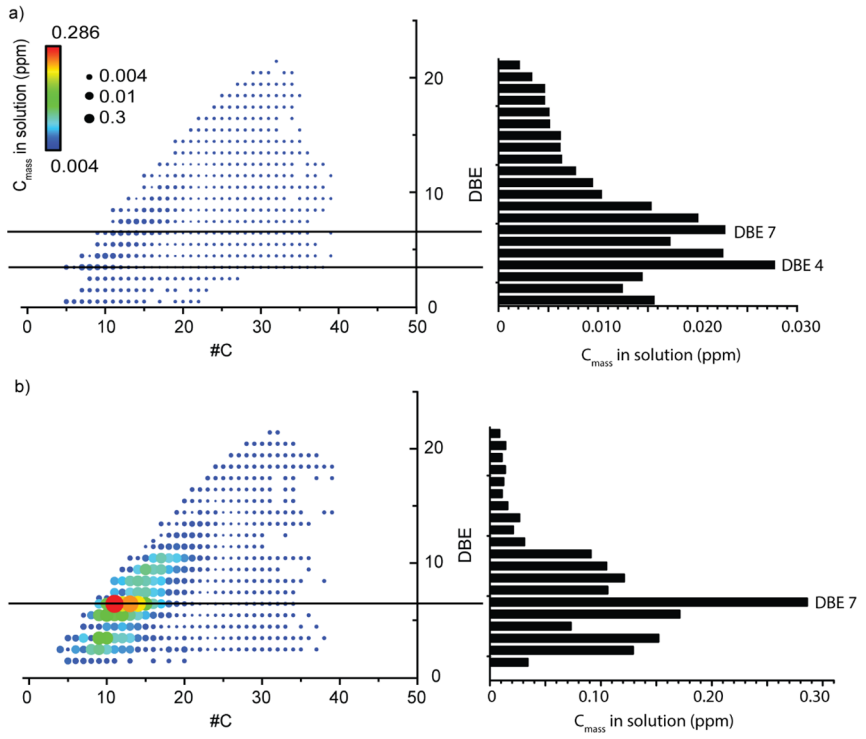


**Figure 5.** Plot of DBE vs the carbon number and the DBE distribution as a function of $C_{mass}$ in solution (ppm N) for (a) $N_1$-containing species and (b) $N_2$-containing species. The color map represents the mass concentration in solution (ppm N) of each ion observed in both classes.

range of the detector. A too-high concentration range could lead to nonlinear response (Figure S8).

Figure 4b presents the mass spectrum obtained via ESI(+)-FTICR for the SAM addition in the case of plastic pyrolysis oil. The insets are enlarged views of the mass spectrum at $m/z$ 145.076025 (Figure 4c) and $m/z$ 186.127726 (Figure 4d), corresponding to the signals of protonated 2-methylquinoxaline and 2-butylquinoline, respectively. Plots of the signal intensity as a function of the concentration of the standards are also represented. In both cases, a linear correlation was obtained that followed the equation intensity = $a \times C_{mass} + b$. As the starting sample contains the compound to be quantified, the calibration line does not pass through the origin point. However, the $x$-intercept yields the analyte concentration (represented by stars in Figure 4c and d). Coefficient of determination ($R^2$) values of 0.9784 and 0.9978 for 2-



https://doi.org/10.1021/acsomega.2c01114
ACS Omega 2022, 7, 19428−19436

Table 1. Results of the SAM for both the $N_1$ (with 2-Butylquinoline) and $N_2$ (with 2-Methylquinoxaline) Classes

| | 2-butylquinoline | | | | | |
|---|---|---|---|---|---|---|
| | replicate 1 | replicate 2 | replicate 3 | average | standard deviation | relative standard deviation |
| $C_{mass(solution)}$(solution) (ppm) | 0.33 | 0.36 | 0.37 | 0.35 | 0.022 | 6.23% |
| $C_{mass}$(oil) (ppm) | 568.75 | 622.85 | 643.31 | 611.64 | 38.52 | 6.30% |
| | 2-methylquinoxaline | | | | | |
| | replicate 1 | replicate 2 | replicate 3 | average | standard deviation | relative standard deviation |
| $C_{mass}$(solution) (ppm) | 0.51 | 0.50 | 0.45 | 0.4 | 0.038 | 7.63% |
| $C_{mass}$(oil) (ppm) | 899.95 | 879.79 | 778.22 | 852.70 | 65.24 | 7.65% |

methylquinoxaline and 2-butylquinoline, respectively, confirm the reliability of the obtained linear correlation. Besides, the equations are different. The slope is higher with this last standard, indicating the response factor is different between the $N_1$- and $N_2$-containing species. Indeed, a molecule containing two basic nitrogen atoms is more likely to be ionized and therefore has a higher response factor than a molecule containing a single basic nitrogen atom. In this case, this means that for the same concentration the signal of a $N_2$-containing species will be higher than signal of a $N_1$-containing species. Both 2-methylquinoxaline and 2-butylquinoline compounds were present in the same concentration in the plastic pyrolysis oil (about 0.018 ppm), whereas their intensities were set to 39 175 400 and 159 698 208, respectively (a factor of four).

As the SAM is not applicable to all compounds, the equation obtained after linear regression was conserved and adapted for all $N_1$- and $N_2$-containing species. Different calculation steps are required to recover the concentrations of all $N_1$- and $N_2$-containing species. They are reported in the Table S2. For the calculation, only the $m/z$ values and corresponding intensities of all compounds in such classes were conserved. Classes were studied separately. For example, the $N_2$ class was kept for the quantification by 2-methylquinoxaline, and the $N_1$ class was kept for the quantification by 2-butylquinoline. Using the equation obtained by linear regression (Figure 5a), the mass concentration ($C_{mass}$) of each signal was retrieved, and the values are reported in the third column of Table S2. However, the elemental content of the oil given in the introduction part (1797 ppm) was in terms of the nitrogen mass concentration. It is therefore necessary to convert the concentration previously obtained in mass to the nitrogen mass concentration. For that, the percentage of nitrogen in each ion (% N in ion) was calculated using the mass of nitrogen and the $m/z$ value (fourth column of Table S2). The mass concentration in N ($C_{mass}$ in N) was obtained by multiplying both $C_{mass}$ and % N in ion (fifth column of Table S2). The sum of all $C_{mass}$ values in the nitrogen-containing species gave the $C_{mass}$ in the analyzed plastic pyrolysis solution as 0.5 mg $mL^{-1}$ for classes chosen.

The last step is to incorporate the dilution factor. The final concentration of nitrogen in the pyrolysis oil ($C_{mass}$ oil) was obtained using eq 2, which takes into account the dilution factor (DF), the $C_{mass}$ in solution (ppm), the density of the solvent used for the preparation of stock solution (g $cm^{-3}$), and the concentration of stock solution (g $mL^{-1}$). In our case, the dilution factor was 10, the solvent used was toluene with a density of 0.867 g $cm^{-3}$, and the concentration of the stock solution was 0.005 g $mL^{-1}$.

$$C_{mass}(\text{oil}) = \text{DF} \times \frac{C_{mass}(\text{solution}) \times \text{density}}{C_{\text{stock solution}}} \quad (2)$$

Table 1 presents results of the SAM for the $N_1$ and $N_2$ classes obtained for each replicate. $N_1$- and $N_2$-containing species represent a total concentration of 1464.3 ppm, with an average of 852.7 ppm $N_2$-containing species and 611.6 ppm $N_1$-containing species. The obtained values have low standard deviations (less than 10%), showing the reproducibility of the experiments. Interestingly, the obtained value (1464.3 ppm) is very close to the concentration obtained by elemental analysis (1500 ppm), confirming the validity of the semiquantification approach despite the approximation done in the response factor. It is important to note that a lot of variability due to other structural differences, such as the total number of carbon atoms, the length of the aliphatic chains, and the positions of the double bonds, could be observed, especially in ESI.[53] The choice of the standard is therefore very important and can significantly distort the final results.

To illustrate the results of the semiquantification, DBE versus carbon number plots and the distribution of the DBE as a function of the mass concentration in solution (ppm) of $N_1$ and $N_2$ are given in Figure 5a and b, respectively. The color map used represents the relative intensity of $C_{mass}$ in solution (ppm) for each ion observed in both classes. We can compare these plots with the DBE versus carbon number plots representing the $N_1$ and $N_2$ ionized species given in Figure 1b and c, respectively. As expected, both distributions were retrieved according to the SAM calculations based on the intensity of each ion. In addition, it is emphasized that the $N_2$-containing species are more present in the plastic oil than the $N_1$-containing species. Their ionization is certainly more important, but the semiquantification also shows their higher quantity in the mixture.

The present approach could be used with other complex organic matter. For instance, microalgae-based bio-oils contain a significant amount of nitrogen-containing species that could be quantified with similar approach to improve the refining processes.[54]

## CONCLUSION

To meet the challenge of analyzing a complex matrix, IRMPD fragmentation and SAM were used with FTICR-MS for the identification and semiquantification of nitrogen-containing species in a pyrolysis plastic oil. Tandem mass spectrometry using a high in-cell resolution for selection and IRMPD generate both extensive fragmentation with a high resolving power and a mass accuracy adapted to the characterization of the structural core and many diagnostic fragments for isomer differentiation. This allowed us to propose molecular structures for use as internal standards consistent with our experimental


https://doi.org/10.1021/acsomega.2c01114
ACS Omega 2022, 7, 19428−19436

data. The semiquantification of the $N_1$ and $N_2$ compound classes in complex matrices was demonstrated for the first time via direct infusion FTICR thanks to the SAM. Interestingly, the global amount of nitrogen-containing species is consistent with the elemental analysis results, which in both cases was shown to be about 1500 ppm nitrogen. The coupling of both tandem mass spectrometry and SAM appears to be a powerful tool for the qualitative and quantitative analysis of complex matrices.

## ■ ASSOCIATED CONTENT

### Supporting Information

The Supporting Information is available free of charge at https://pubs.acs.org/doi/10.1021/acsomega.2c01114.

Comparison of the quadrupole selection and the in-cell selection for $C_{10}H_{14}N^+$ and $C_{14}H_{16}N^+$, discussions of the fragmentation of these both ions, and mass spectra (PDF)

## ■ AUTHOR INFORMATION


### Corresponding Author

**Carlos Afonso** − *UMR 6014 et FR 3038, COBRA, INSA de Rouen, IRCOF, Université de Rouen, Normandie Université, CNRS, Rouen 76130, France; International Joint Laboratory − iC2MC: Complex Matrices Molecular Characterization, TotalEnergies Research and Technology Gonfreville, Harfleur 76700, France;* orcid.org/0000-0002-2406-5664; Email: carlos.afonso@univ-rouen.fr

### Authors

**Charlotte Mase** − *UMR 6014 et FR 3038, COBRA, INSA de Rouen, IRCOF, Université de Rouen, Normandie Université, CNRS, Rouen 76130, France; TotalEnergies OneTech, TotalEnergies Research and Technology Gonfreville, Harfleur 76700, France; International Joint Laboratory − iC2MC: Complex Matrices Molecular Characterization, TotalEnergies Research and Technology Gonfreville, Harfleur 76700, France*

**Julien Florent Maillard** − *UMR 6014 et FR 3038, COBRA, INSA de Rouen, IRCOF, Université de Rouen, Normandie Université, CNRS, Rouen 76130, France; International Joint Laboratory − iC2MC: Complex Matrices Molecular Characterization, TotalEnergies Research and Technology Gonfreville, Harfleur 76700, France;* orcid.org/0000-0001-5620-8474

**Benoit Paupy** − *TotalEnergies OneTech, TotalEnergies Research and Technology Gonfreville, Harfleur 76700, France; International Joint Laboratory − iC2MC: Complex Matrices Molecular Characterization, TotalEnergies Research and Technology Gonfreville, Harfleur 76700, France*

**Marie Hubert-Roux** − *UMR 6014 et FR 3038, COBRA, INSA de Rouen, IRCOF, Université de Rouen, Normandie Université, CNRS, Rouen 76130, France; International Joint Laboratory − iC2MC: Complex Matrices Molecular Characterization, TotalEnergies Research and Technology Gonfreville, Harfleur 76700, France*

**Pierre Giusti** − *UMR 6014 et FR 3038, COBRA, INSA de Rouen, IRCOF, Université de Rouen, Normandie Université, CNRS, Rouen 76130, France; TotalEnergies OneTech, TotalEnergies Research and Technology Gonfreville, Harfleur 76700, France; International Joint Laboratory − iC2MC: Complex Matrices Molecular Characterization, TotalEnergies Research and Technology Gonfreville, Harfleur 76700, France;* orcid.org/0000-0002-9569-3158

Complete contact information is available at: https://pubs.acs.org/10.1021/acsomega.2c01114


### Notes

The authors declare no competing financial interest.

## ■ ACKNOWLEDGMENTS

This work has been partially supported by University of Rouen Normandy, INSA Rouen Normandy, the European Regional Development Fund (ERDF) no. HN0001343, Labex SynOrg (Grant ANR-11-LABX-0029), Carnot Institute I2C, the Graduate School for Research XL-Chem (Grant ANR-18-EURE-0020), the European Union's Horizon 2020 Research Infrastructures program (Grant Agreement 731077), and Région Normandie. Access to the Centre National de la Recherche Scientifique (CNRS) FTICR research infrastructure Infranalytics (FR2054) is gratefully acknowledged.

## ■ REFERENCES


(1) Geyer, R.; Jambeck, J. R.; Law, K. L. Production, use, and fate of all plastics ever made. *Phys. Rev.* **2017**, *3* (7), No. e1700782.

(2) Kumar, S.; Singh, E.; Mishra, R.; Kumar, A.; Caucci, S. Utilization of Plastic Wastes for Sustainable Environmental Management: A Review. *ChemSusChem* **2021**, *14* (19), 3985−4006.

(3) Mastellone, M. L. Technical description and performance evaluation of different packaging plastic waste management's systems in a circular economy perspective. *Sci. Total Environ.* **2020**, *718*, 137233.

(4) Robaina, M.; Murillo, K.; Rocha, E.; Villar, J. Circular economy in plastic waste - Efficiency analysis of European countries. *Sci. Total Environ.* **2020**, *730*, 139038.

(5) Huysman, S.; De Schaepmeester, J.; Ragaert, K.; Dewulf, J.; De Meester, S. Performance indicators for a circular economy: A case study on post-industrial plastic waste. *Resour. Conserv. Recycl* **2017**, *120*, 46−54.

(6) Payne, J.; McKeown, P.; Jones, M. D. A circular economy approach to plastic waste. *Polym. Degrad. Stab.* **2019**, *165*, 170−181.

(7) Al-Salem, S. M.; Antelava, A.; Constantinou, A.; Manos, G.; Dutta, A. A review on thermal and catalytic pyrolysis of plastic solid waste (PSW). *J. Environ. Manage* **2017**, *197*, 177−198.

(8) Antelava, A.; Jablonska, N.; Constantinou, A.; Manos, G.; Salaudeen, S. A.; Dutta, A.; Al-Salem, S. M. Energy Potential of Plastic Waste Valorization: A Short Comparative Assessment of Pyrolysis versus Gasification. *Energy Fuels* **2021**, *35* (5), 3558−3571.

(9) Kasar, P.; Sharma, D. K.; Ahmaruzzaman, M. Thermal and catalytic decomposition of waste plastics and its co-processing with petroleum residue through pyrolysis process. *J. Clean. Prod* **2020**, *265*, 121639.

(10) Qureshi, M. S.; Oasmaa, A.; Pihkola, H.; Deviatkin, I.; Tenhunen, A.; Mannila, J.; Minkkinen, H.; Pohjakallio, M.; Laine-Ylijoki, J. Pyrolysis of plastic waste: Opportunities and challenges. *J. Anal. Appl. Pyrolysis* **2020**, *152*, 104804.

(11) Sharuddin, S. D. A.; Abnisa, F.; Daud, W. M. A. W.; Aroua, M. K. Pyrolysis of plastic waste for liquid fuel production as prospective energy resource. *IOP Conf. Ser.: Meter. Sci. Eng.* **2018**, *334*, No. 012001.

(12) Ware, R. L.; Rowland, S. M.; Rodgers, R. P.; Marshall, A. G. Advanced Chemical Characterization of Pyrolysis Oils from Landfill Waste, Recycled Plastics, and Forestry Residue. *Energy Fuels* **2017**, *31* (8), 8210−8216.

(13) Sandes, L. V. O.; Vieira, W. T.; Albuquerque, A. A.; Bezerra, P. X. O.; Ribeiro, L. M. O.; Carvalho, S. H. V.; Soletti, J. I.; Bispo, M. D. Pyrolysis of Lignocellulosic Waste from Second-Generation Ethanol Industry. *Sugar Tech.* **2021**, *23*, 615.

(14) Varma, A. K.; Thakur, L. S.; Shankar, R.; Mondal, P. Pyrolysis of wood sawdust: Effects of process parameters on products yield and characterization of products. *Waste Manag* **2019**, *89*, 224−235.
(15) Staš, M.; Chudoba, J.; Kubička, D.; Blažek, J.; Pospíšil, M. Petroleomic Characterization of Pyrolysis Bio-oils: A Review. *Energy Fuels* **2017**, *31* (10), 10283−10299.
(16) Dhahak, A.; Carre, V.; Aubriet, F.; Mauviel, G.; Burkle-Vitzthum, V. Analysis of Products Obtained from Slow Pyrolysis of Poly(ethylene terephthalate) by Fourier Transform Ion Cyclotron Resonance Mass Spectrometry Coupled to Electrospray Ionization (ESI) and Laser Desorption Ionization (LDI). *Ind. Eng. Chem. Res.* **2020**, *59* (4), 1495−1504.
(17) Dimitrov, N.; Kratofil Krehula, L.; Ptiček Siročić, A.; Hrnjak-Murgić, Z. Analysis of recycled PET bottles products by pyrolysis-gas chromatography. *Polym. Degrad. Stab.* **2013**, *98* (5), 972−979.
(18) Miskolczi, N.; Bartha, L.; Angyal, A. Pyrolysis of Polyvinyl Chloride (PVC)-Containing Mixed Plastic Wastes for Recovery of Hydrocarbons. *Energy Fuels* **2009**, *23* (5), 2743−2749.
(19) Çit, İ.; Sınağ, A.; Yumak, T.; Uçar, S.; Mısırlıoğlu, Z.; Canel, M. Comparative pyrolysis of polyolefins (PP and LDPE) and PET. *Polym. Bull.* **2010**, *64* (8), 817−834.
(20) Williams, P. T.; Williams, E. A. Interaction of Plastics in Mixed-Plastics Pyrolysis. *Energy Fuels* **1999**, *13* (1), 188−196.
(21) Williams, P. T.; Slaney, E. Analysis of products from the pyrolysis and liquefaction of single plastics and waste plastic mixtures. *Resour. Conserv. Recycl* **2007**, *51* (4), 754−769.
(22) Lopez, A.; de Marco, I.; Caballero, B. M.; Laresgoiti, M. F.; Adrados, A. Pyrolysis of municipal plastic wastes: Influence of raw material composition. *Waste Manag* **2010**, *30* (4), 620−7.
(23) Toraman, H. E.; Dijkmans, T.; Djokic, M. R.; Van Geem, K. M.; Marin, G. B. Detailed compositional characterization of plastic waste pyrolysis oil by comprehensive two-dimensional gas-chromatography coupled to multiple detectors. *J. Chromatogr. A* **2014**, *1359*, 237−46.
(24) Zhou, H.; Wu, C.; Onwudili, J. A.; Meng, A.; Zhang, Y.; Williams, P. T. Polycyclic aromatic hydrocarbons (PAH) formation from the pyrolysis of different municipal solid waste fractions. *Waste Manag* **2015**, *36*, 136−46.
(25) Ware, R. L.; Rowland, S. M.; Lu, J.; Rodgers, R. P.; Marshall, A. G. Compositional and Structural Analysis of Silica Gel Fractions from Municipal Waste Pyrolysis Oils. *Energy Fuels* **2018**, *32* (7), 7752−7761.
(26) Singh, R. K.; Ruj, B.; Sadhukhan, A. K.; Gupta, P. Impact of fast and slow pyrolysis on the degradation of mixed plastic waste: Product yield analysis and their characterization. *J. Energy Inst* **2019**, *92* (6), 1647−1657.
(27) Wu, J.; Chen, T.; Luo, X.; Han, D.; Wang, Z.; Wu, J. TG/FTIR analysis on co-pyrolysis behavior of PE, PVC and PS. *Waste Manag* **2014**, *34* (3), 676−82.
(28) Dhahak, A.; Grimmer, C.; Neumann, A.; Ruger, C.; Sklorz, M.; Streibel, T.; Zimmermann, R.; Mauviel, G.; Burkle-Vitzthum, V. Real time monitoring of slow pyrolysis of polyethylene terephthalate (PET) by different mass spectrometric techniques. *Waste Manag* **2020**, *106*, 226−239.
(29) Mase, C.; Maillard, J. F.; Paupy, B.; Farenc, M.; Adam, C.; Hubert-Roux, M.; Afonso, C.; Giusti, P. Molecular Characterization of a Mixed Plastic Pyrolysis Oil from Municipal Wastes by Direct Infusion Fourier Transform Ion Cyclotron Resonance Mass Spectrometry. *Energy Fuels* **2021**, *35*, 14828.
(30) Cody, R. B.; Burnier, R. C.; Freiser, B. S. Collision-induced dissociation with fourier transform mass spectrometry. *Anal. Chem.* **1982**, *54*, 96−101.
(31) Little, D. P.; Speir, J. P.; Senko, M. W.; O'Connor, P. B.; McLafferty, F. W. Infrared multiphoton dissociation of large multiply charged ions for biomolecule sequencing. *Anal. Chem.* **1994**, *66* (18), 2809.
(32) Mabud, M. A.; Dekrey, M. J.; Graham Cooks, R. Surface-induced dissociation of molecular ions. *IMSPF8* **1985**, *67* (3), 285−294.
(33) Qi, Y.; Volmer, D. A. Electron-based fragmentation methods in mass spectrometry: An overview. *Mass Spectrom. Rev.* **2017**, *36* (1), 4−15.
(34) Zubarev, R. A. Electron-capture dissociation tandem mass spectrometry. *Curr. Opin. Biotechnol* **2004**, *15* (1), 12−6.
(35) Neumann, A.; Chacón-Patiño, M. L.; Rodgers, R. P.; Rüger, C. P.; Zimmermann, R. Investigation of Island/Single-Core- and Archipelago/Multicore-Enriched Asphaltenes and Their Solubility Fractions by Thermal Analysis Coupled with High-Resolution Fourier Transform Ion Cyclotron Resonance Mass Spectrometry. *Energy Fuels* **2021**, *35* (5), 3808−3824.
(36) Maillard, J.; Schmitz-Afonso, I.; Gautier, T.; Afonso, C.; Carrasco, N. Suggested plausible structures for Titan's haze analogs using tandem mass spectrometry. *Icarus* **2021**, *358*, 114181.
(37) Vulpius, T.; Houriet, R. External phase shift ion ejection in fourier transform ion cyclotron resonance spectrometry. *IMSPF8* **1989**, *88* (2−3), 283−290.
(38) Nilsson, L. B.; Eklund, G. Direct quantification in bioanalytical LC-MS/MS using internal calibration via analyte/stable isotope ratio. *J. Pharm. Biomed Anal* **2007**, *43* (3), 1094−9.
(39) Nunes, M. A.; Voss, M.; Corazza, G.; Flores, E. M.; Dressler, V. L. External calibration strategy for trace element quantification in botanical samples by LA-ICP-MS using filter paper. *Anal. Chim. Acta* **2016**, *905*, 51−7.
(40) Garrido Frenich, A.; Martinez Vidal, J. L.; Fernandez Moreno, J. L.; Romero-Gonzalez, R. Compensation for matrix effects in gas chromatography-tandem mass spectrometry using a single point standard addition. *J. Chromatogr. A* **2009**, *1216* (23), 4798−808.
(41) Hertzog, J.; Mase, C.; Hubert-Roux, M.; Afonso, C.; Giusti, P.; Barrère-Mangote, C. Characterization of Heavy Products from Lignocellulosic Biomass Pyrolysis by Chromatography and Fourier Transform Mass Spectrometry: A Review. *Energy Fuels* **2021**, *35*, 17979.
(42) Buss, W.; Hertzog, J.; Pietrzyk, J.; Carré, V.; Mackay, C. L.; Aubriet, F.; Mašek, O. Comparison of Pyrolysis Liquids from Continuous and Batch Biochar Production—Influence of Feedstock Evidenced by FTICR MS. *Energies* **2021**, *14* (1), 9.
(43) Castilla, C.; Ruger, C. P.; Marcotte, S.; Lavanant, H.; Afonso, C. Direct Inlet Probe Atmospheric Pressure Photo and Chemical Ionization Coupled to Ultrahigh Resolution Mass Spectrometry for the Description of Lignocellulosic Biomass. *J. Am. Soc. Mass. Spectrom* **2020**, *31* (4), 822−831.
(44) Maillard, J.; Carrasco, N.; Schmitz-Afonso, I.; Gautier, T.; Afonso, C. Comparison of soluble and insoluble organic matter in analogues of Titan's aerosols. *EPSL* **2018**, *495*, 185−191.
(45) Rodgers, R. P.; McKenna, A. M. Petroleum analysis. *Anal. Chem.* **2011**, *83* (12), 4665−87.
(46) Hughey, C. A.; Hendrickson, C. L.; Rodgers, R. P.; Marshall, A. G. Elemental Composition Analysis of Processed and Unprocessed Diesel Fuel by Electrospray Ionization Fourier Transform Ion Cyclotron Resonance Mass Spectrometry. *Energy Fuels* **2001**, *15* (5), 1186−1193.
(47) Purcell, J. M.; Rodgers, R. P.; Hendrickson, C. L.; Marshall, A. G. Speciation of nitrogen containing aromatics by atmospheric pressure photoionization or electrospray ionization fourier transform ion cyclotron resonance mass spectrometry. *J. Am. Soc. Mass. Spectrom* **2007**, *18* (7), 1265−73.
(48) Le Maître, J.; Paupy, B.; Hubert-Roux, M.; Marceau, S.; Rüger, C.; Afonso, C.; Giusti, P. Structural Analysis of Neutral Nitrogen Compounds Refractory to the Hydrodenitrogenation Process of Heavy Oil Fractions by HighResolution Tandem Mass Spectrometry and Ion Mobility−Mass Spectrometry. *Energy Fuels* **2020**, *34*, 9328.
(49) Farenc, M.; Paupy, B.; Marceau, S.; Riches, E.; Afonso, C.; Giusti, P. Effective Ion Mobility Peak Width as a New Isomeric Descriptor for the Untargeted Analysis of Complex Mixtures Using Ion Mobility-Mass Spectrometry. *J. Am. Soc. Mass. Spectrom* **2017**, *28* (11), 2476−2482.
(50) Ceba, M. R.; Linares, C. J.; Barrero, F. A.; Campaña, A. M. G.; Rodríguez, L. C. Validation of an Analytical Instrumental Method by


https://doi.org/10.1021/acsomega.2c01114
*ACS Omega* 2022, 7, 19428−19436

Standard Addition Methodology. *J. AOAC Int.* **1995**, *78* (2), 471−476.
(51) Saxberg, B. E. H.; Kowalski, B. R. Generalized standard addition method. *Anal. Chem.* **1979**, *51* (7), 1031−1038.
(52) Ellison, S. L.; Thompson, M. Standard additions: myth and reality. *Analyst* **2008**, *133* (8), 992−7.
(53) Hindle, R.; Noestheden, M.; Peru, K.; Headley, J. Quantitative analysis of naphthenic acids in water by liquid chromatography-accurate mass time-of-flight mass spectrometry. *J. Chromatogr. A* **2013**, *1286*, 166−74.
(54) Barrère-Mangote, C.; Roubaud, A.; Bouyssiere, B.; Maillard, J.; Hertzog, J.; Maître, J. L.; Hubert-Roux, M.; Sassi, J.-F.; Afonso, C.; Giusti, P. Study of Biocrudes Obtained via Hydrothermal Liquefaction (HTL) of Wild Alga Consortium under Different Conditions. *Processes* **2021**, *9* (9), 1494.



https://doi.org/10.1021/acsomega.2c01114
*ACS Omega* 2022, 7, 19428−19436